

# Effects of pressure and temperature on the carrier transports in organic crystal: A first-principles study

L. J. Wang, Q. K. Li, and Z. Shuai

Citation: *The Journal of Chemical Physics* **128**, 194706 (2008); doi: 10.1063/1.2918276

View online: <https://doi.org/10.1063/1.2918276>

View Table of Contents: <http://aip.scitation.org/toc/jcp/128/19>

Published by the [American Institute of Physics](#)

---

## Articles you may be interested in

[Roles of inter- and intramolecular vibrations and band-hopping crossover in the charge transport in naphthalene crystal](#)

*The Journal of Chemical Physics* **127**, 044506 (2007); 10.1063/1.2751191

[Temperature dependent activation energy for electron transfer between biological molecules](#)

*The Journal of Chemical Physics* **64**, 4860 (1976); 10.1063/1.432142

[Quantized Hamiltonian dynamics captures the low-temperature regime of charge transport in molecular crystals](#)

*The Journal of Chemical Physics* **139**, 174109 (2013); 10.1063/1.4828863

[Mixed quantum-classical simulations of charge transport in organic materials: Numerical benchmark of the Su-Schrieffer-Heeger model](#)

*The Journal of Chemical Physics* **134**, 244116 (2011); 10.1063/1.3604561

[Charge transfer rates in organic semiconductors beyond first-order perturbation: From weak to strong coupling regimes](#)

*The Journal of Chemical Physics* **130**, 024704 (2009); 10.1063/1.3055519

[Ab initio theory of charge-carrier conduction in ultrapure organic crystals](#)

*Applied Physics Letters* **85**, 1535 (2004); 10.1063/1.1776335

---

PHYSICS TODAY

WHITEPAPERS

### ADVANCED LIGHT CURE ADHESIVES

Take a closer look at what these environmentally friendly adhesive systems can do

READ NOW

PRESENTED BY  
 **MASTERBOND**  
ADHESIVES | SEALANTS | COATINGS

# Effects of pressure and temperature on the carrier transports in organic crystal: A first-principles study

L. J. Wang,<sup>1</sup> Q. K. Li,<sup>1,2</sup> and Z. Shuai<sup>1,2,a)</sup><sup>1</sup>Key Laboratory of Organic Solids, Beijing National Laboratory for Molecular Sciences (BNLMS), Institute of Chemistry, Chinese Academy of Sciences, 100080 Beijing, People's Republic of China<sup>2</sup>Department of Chemistry, Tsinghua University, 100084 Beijing, People's Republic of China

(Received 17 January 2008; accepted 3 April 2008; published online 16 May 2008)

By employing density-functional theory coupled with Holstein–Peierls model, we investigate the pressure and temperature dependence of the hole and electron mobilities in naphthalene single crystal from atmospheric pressure up to 2.1 GPa (at room temperature) and from 5 to 296 K (at ambient pressure). It is found that the pressure reduces the electron-phonon coupling strength and enhances the mobilities. Importantly, we point out that only when temperature-dependent structure modifications are taken into account can one better describe the temperature-dependent transport behavior. Especially, the band to hopping crossover transition temperature for the electron transport in the  $c'$ -axis is calculated to be around 153 K, which is close to the experimental result of between 100 and 150 K. If this temperature-dependent structure modifications were neglected, the transition temperature would be only about 23 K, as previously obtained [L. J. Wang *et al.*, J. Chem. Phys. **127**, 044506 (2007)]. © 2008 American Institute of Physics. [DOI: 10.1063/1.2918276]

## I. INTRODUCTION

Organic semiconductors have been applied in light-emitting diodes, thin-film transistors, and photovoltaic cells.<sup>1–7</sup> The charge carrier mobilities critically influence their performance.<sup>8</sup> Remarkable progresses in increasing the charge mobility have been achieved in recent years. Experimentally, the room-temperature mobilities of pentacene and rubrene have surpassed amorphous Si.<sup>5,9,10</sup> Various theoretical models have been proposed.<sup>11–19</sup> However, a complete understanding of the transport mechanism is still lacking.<sup>8</sup>

Pressure is a useful tool to uncover the underlying transport physics for organic materials. Both increasing pressure and lowering temperature result in a volume decrease, which influence both the electronic structure and the electron-phonon interaction, and eventually the carrier mobility.<sup>8,20</sup> The pressure variation of the mobilities involves the structure dependence only, while the effect of temperature involves a mixed dependence on both temperature and structure.<sup>21</sup> A detailed study of these two effects can shed light in better understanding the intrinsic transport mechanism. Experimentally, Rang *et al.* observed a linear increase in field-effect mobility with increasing pressure ( $\mu \propto P$ ) in tetracene, pentacene, and rubrene.<sup>20,22</sup> In single organic crystal, the charge carrier mobilities generally decrease with temperature according to a power law ( $\mu \propto T^{-n}$ ).<sup>8,23</sup> The purpose of this work is to employ the first-principles calculation to investigate the pressure dependence of mobilities first, and then to see how the temperature-dependent structure modification influences the carrier mobility in organic materials.

Following the pioneering work of Holstein,<sup>11</sup> a small-polaron charge transport theory based on a Holstein–Peierls Hamiltonian has been recently proposed by Bobbert and

coworkers.<sup>14,24,25</sup> The model contains both the bandlike and the hopping terms, which has been shown to reproduce the experimental temperature-dependent mobilities of organic semiconductor naphthalene single crystal.<sup>14,26(a)</sup> It is found that the intermolecular vibrational modes play much more important role than the intramolecular vibrations.<sup>26(a)</sup> On the other hand, several experiments have been carried out to investigate the pressure effects on charge transport. Both lattice constants<sup>27–33</sup> and phonon frequencies<sup>21,34–36</sup> have been found to be sensitive to temperature and pressure.

In this work, starting from the experimentally determined pressure-/temperature-dependent structures, we study the structure-transport relationships by means of the Holstein–Peierls model projected by density-functional theory (DFT) calculations. The relationships between both hole and electron mobilities with pressure and temperature have been investigated.

## II. THEORETICAL METHODOLOGY

The Holstein–Peierls Hamiltonian reads<sup>14,26(a)</sup>

$$H = \sum_{mn} \varepsilon_{mn} a_m^+ a_n + \sum_{\lambda} \hbar \omega_{\lambda} \left( b_{\lambda}^+ b_{\lambda} + \frac{1}{2} \right) + \sum_{mn\lambda} \hbar \omega_{\lambda} g_{\lambda mn} (b_{\lambda}^+ + b_{-\lambda}) a_m^+ a_n. \quad (1)$$

Here  $a_n^+$  ( $a_n$ ) represents creating (annihilating) a charge carrier at site (molecule)  $n$ , and  $b_{\lambda}^+$  ( $b_{\lambda}$ ) represents creating (annihilating) a phonon indexed as  $\lambda$ .  $\varepsilon_{mn}$  is the transfer integral between sites  $m$  and  $n$ ,  $\omega_{\lambda}$  is the frequency of phonon  $\lambda$ , and  $g_{\lambda mn}$  is the electron-phonon coupling constant between phonon mode  $\lambda$  in the charge transfer path  $m \rightarrow n$ . All the coupling constants  $g_{\lambda mn}$ , including both local ( $m=n$ ) and nonlocal ( $m \neq n$ ) parts for inter- ( $\lambda \in$  intermolecular) and

<sup>a)</sup>Electronic mail: zgshuai@iccas.ac.cn.

intramolecular ( $\lambda \in$  intramolecular) vibrations, have been taken into consideration.<sup>26(a)</sup>

Starting from the Holstein–Peierls Hamiltonian, the conductivity can be evaluated with the Kubo formalism of linear response theory with a current-current correlation function.<sup>14,25</sup> The temperature-dependent mobility can be expressed as

$$\begin{aligned} \mu_{\alpha}(T) &= \frac{e_0}{2k_B T \hbar^2} \\ &\times \sum_{n \neq m} (R_{am} - R_{an})^2 \int_{-\infty}^{\infty} dt e^{-\Gamma^2 t^2 - \sum_{\lambda} 2G_{\lambda} [1 + 2N_{\lambda} - \Phi_{\lambda}(t)]} \\ &\times \left[ \varepsilon_{mn}^2 + (\varepsilon_{mn} - \Delta_{mn})^2 + \frac{1}{2} \sum_q (\hbar \omega_q g_{qmn})^2 \Phi_q(t) \right], \quad (2) \end{aligned}$$

where  $G_{\lambda} = g_{\lambda mn}^2 + \frac{1}{2} \sum_{k \neq m} g_{\lambda mk}^2$  is the effective electron-phonon coupling constant,  $N_{\lambda} = 1 / (e^{\hbar \omega_{\lambda} / k_B T} - 1)$  is the phonon occupation number,  $\Phi_{\lambda}(t) = (1 + N_{\lambda}) e^{-i\omega_{\lambda} t} + N_{\lambda} e^{i\omega_{\lambda} t}$  is called the incoherent scattering factor, and  $\Delta_{mn} = \frac{1}{2} \sum_{\lambda} \hbar \omega_{\lambda} [g_{\lambda mn} (g_{\lambda mm} + g_{\lambda nn}) + \frac{1}{2} \sum_{k \neq m, n} g_{\lambda mk} g_{\lambda kn}]$ .<sup>14</sup>  $R_{am}$  is the Cartesian coordinate of lattice site  $m$  in the  $a$ th direction.  $\Gamma$  is a phenomenological parameter for inhomogeneous line broadening, which is typically taken to be very small (less than a meV).<sup>14,25,26(a)</sup>

The local and nonlocal contributions to the mobility can be separated by defining<sup>26(a)</sup>

$$\mu_{\alpha} = \mu_{\alpha}^{\text{local}} + \mu_{\alpha}^{\text{nonlocal}}, \quad (3)$$

where

$$\mu_{\alpha}^{\text{local}} \equiv \frac{e_0}{2k_B \hbar^2} \sum_{n \neq m} (R_{am} - R_{an})^2 [\varepsilon_{mn}^2 + (\varepsilon_{mn} - \Delta_{mn})^2] \frac{1}{T} \int_{-\infty}^{\infty} dt e^{\sum_{\lambda} -2G_{\lambda} (1 + 2N_{\lambda}(T)) (1 - \cos \omega_{\lambda} t) - \Gamma^2 t^2} \cos \left( \sum_{\lambda} 2G_{\lambda} \sin \omega_{\lambda} t \right), \quad (4)$$

$$\begin{aligned} \mu_{\alpha}^{\text{nonlocal}} &\equiv \frac{e_0}{2k_B \hbar^2} \sum_{n \neq m} (R_{am} - R_{an})^2 \frac{1}{2} \hbar \omega_q^2 g_{qmn}^2 \left[ \frac{1}{T} (1 + N_q(T)) \int_{-\infty}^{\infty} dt e^{\sum_{\lambda} -2G_{\lambda} (1 + 2N_{\lambda}(T)) (1 - \cos \omega_{\lambda} t) - \Gamma^2 t^2} \cos \left( \sum_{\lambda} 2G_{\lambda} \sin \omega_{\lambda} t + \omega_q t \right) \right. \\ &\left. + \frac{1}{T} N_q(T) \int_{-\infty}^{\infty} dt e^{\sum_{\lambda} -2G_{\lambda} (1 + 2N_{\lambda}(T)) (1 - \cos \omega_{\lambda} t) - \Gamma^2 t^2} \cos \left( \sum_{\lambda} 2G_{\lambda} \sin \omega_{\lambda} t - \omega_q t \right) \right]. \quad (5) \end{aligned}$$

From our previous study,<sup>26(a)</sup> when the temperature increases, the nonlocal parts start to increase, then level off, and finally slightly decrease with  $T$ . Since this is a basic character of classical Marcus hopping theory,<sup>26(b)</sup> namely, when temperature is increased to overcome the barrier, the exponential function levels off, and then the prefactor of  $T^{-1/2}$  in Marcus formula dominates the (decrease with) temperature behavior, much as the nonlocal parts in this work.<sup>26(a)</sup> Besides, the local part monotonically decreases with  $T$  when the electron-phonon coupling is weak, and has a local minimum in the temperature dependence when the coupling is strong.<sup>12,26(a)</sup> However, at low temperature, the local part always decreases with temperature. Therefore,  $\mu_{\alpha}^{\text{local}}$  and  $\mu_{\alpha}^{\text{nonlocal}}$  correspond to the bandlike and hopping mobilities exactly at low temperature, but the classification becomes blurred at higher temperatures. Furthermore, we should bear in mind that the definite separation of the tunneling part and hopping part in the polaron model is not easy, and even harder in our theory which considers all the electron-phonon coupling constants, including both local and nonlocal parts for inter- and intramolecular vibrations.<sup>8</sup> Although the classification is not clear over all the temperature range, a detailed study of the distributions of the two parts can still help us understand the intrinsic relationship between transport properties and structure.<sup>26(a)</sup>

There are five basic physical quantities in Eq. (2): Tem-

perature  $T$ , structural coordinates  $R_{am}$ , phonon frequencies  $\omega_q$ , transfer integrals  $\varepsilon_{mn}$ , and the electron-phonon coupling constants  $g_{qmn}$ . At given temperature  $T$  and pressure  $P$ , the site coordinates  $R_{am}$  are fixed. The procedures for calculating  $\omega_q$ ,  $\varepsilon_{mn}$ , and  $g_{qmn}$  involve extensive first-principles DFT calculation for both the band structure and the vibration spectrum, and the subsequent projections into a tight-binding model, which have been described in detail elsewhere.<sup>26(a)</sup> Here we only give a brief summary. The phonon frequencies are evaluated from the Hessian matrix only at the  $\Gamma$ -point, namely, the phonon dispersion is neglected due to the limit of computational complexity: Organic crystals usually consist of large unit cell and the intermolecular interactions are weak. The transfer integrals are obtained by fitting the DFT band structure with the tight-binding model

$$\varepsilon(\vec{k}) = \varepsilon_0 + \sum_{\langle ij \rangle} \varepsilon_{ij} e^{-i\vec{k} \cdot \vec{R}_{ij}} \quad (6)$$

both for the highest occupied crystal orbital (HOCO) and the lowest unoccupied crystal orbital (LUCO) energy bands. Only the transfer integrals of the neighbors  $\{mn\} = \{0, a, b, c, ac, ab, abc\}$  with  $R_m - R_n = 0, \pm a, \pm b, \pm c, \pm(a+c), \pm(a/2 \pm b/2)$ , and  $\pm(a/2 \pm b/2 + c)$  (see Fig. 1) are considered in the fitting procedure as the long range intermolecular overlaps are extremely small for organic crystal.<sup>26(a)</sup> The electron-phonon coupling constants are ob-

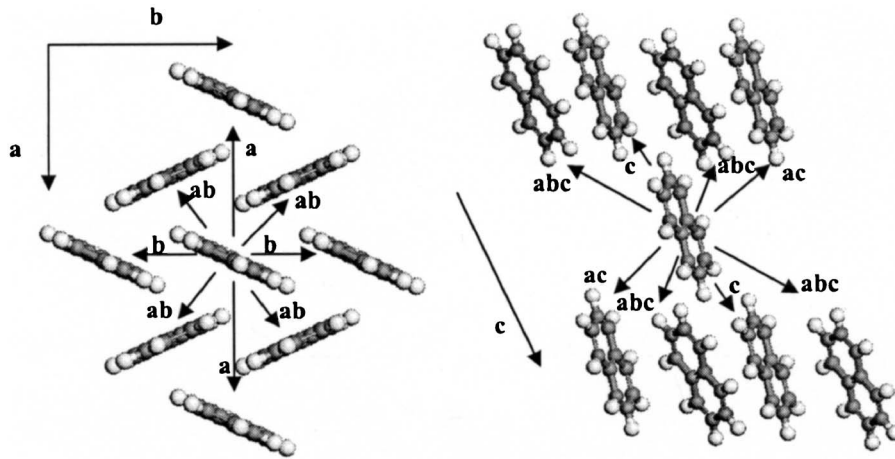


FIG. 1. Labeling of nearest neighbors for intralayer and interlayer of naphthalene crystal.

tained by numerical differentiation of the transfer integrals with respect to the phonon normal coordinates

$$g_{\lambda mn} = \frac{1}{\omega_\lambda \sqrt{\hbar \omega_\lambda}} \frac{\partial \varepsilon_{mn}}{\partial Q_\lambda}. \quad (7)$$

Then the mobility is obtained through Eq. (2).

### III. NUMERICAL RESULTS AND DISCUSSIONS

#### A. Calculation details

All the calculations in this work are performed with the Vienna *ab initio* simulation package<sup>37</sup> (VASP) which has proved to be a power tool for the theoretical study of periodic systems.<sup>38</sup> The Perdew–Burke–Ernzerhof (PBE) exchange–correlation (XC) functional is chosen because it can best describe the weak intermolecular interaction for molecular crystals.<sup>39</sup> The lattice constants are fixed with data from experiment.<sup>8,27,29,30,33</sup> Plane wave kinetic energy cutoff is 600 eV. The optimizations using constrained unit-cell parameters are done until all the atomic forces are less than 0.01 eV/Å. The convergence criterion of the total energy is  $10^{-5}$  eV in the self-consistent field iteration. We choose very small inhomogeneous line broadening factor  $\hbar\Gamma=0.1$  meV, which corresponds to ultrapure crystal.<sup>14</sup> A  $4 \times 4 \times 4$   $k$ -space grid in the first Brillouin zone is used to evaluate the transfer integrals with the band-fitting method.

#### B. Pressure-dependent mobility

To investigate the relationship between mobility and pressure at room temperature, we start with the lattice constants determined by experiment under various pressures (see Table I) to evaluate all the basic quantities in Eq. (2). First, in Fig. 2, we depict the pressure-induced phonon frequency change ratio. It is evident that the most important changes occur at the low-frequency part. Namely, the pressure makes the crystal more solid. The intermolecular interaction is enhanced and then the intermolecular vibration frequency is increased. The calculated results can compare well to the experimental results [shown in the inset of Fig. 2(a)]. This indicates the computational scheme, especially the choice of XC (PBE) functional is reasonable. We depict more explicitly the pressure dependences of the lowest three intermo-

lecular vibrational modes in Fig. 2(b). In fact, the frequency change is related to the unit-cell volume change by the mode-Grüneisen parameter  $\gamma$  defined as

$$\gamma = -d\left(\ln \frac{\omega}{\omega_0}\right) / d\left(\ln \frac{V}{V_0}\right) = d\left(\ln \frac{\omega}{\omega_0}\right) / d\left(\ln \frac{V_0}{V}\right). \quad (8)$$

For the most important intermolecular vibrational mode of  $\omega_0=48.8$  cm<sup>-1</sup>, we made a log-log plot [see Fig. 2(c)] to fit

TABLE I. Lattice parameters of naphthalene crystal at different pressures (at room temperature) and temperatures (at atmospheric pressure) ( $\alpha=90^\circ$ ).

Pressure (GPa)	$a$ (Å)	$b$ (Å)	$c$ (Å)	$\beta$ (deg)
$1.013\ 25E-4^a$	8.235	6.003	8.658	122.92
$0.4^b$	8.0348	5.8899	8.565	123.59
$0.6^b$	7.9948	5.8726	8.542	123.677
$1.0^b$	7.8523	5.8106	8.474	124.027
$2.1^b$	7.6778	5.721	8.395	124.55
Temperature (K)	$a$ (Å)	$b$ (Å)	$c$ (Å)	$\beta$ (deg)
$5^c$	8.0711	5.9272	8.624	124.661
$50^c$	8.0798	5.9303	8.6288	124.582
$92^d$	8.1080	5.9397	8.6472	124.379
$109^d$	8.1224	5.9430	8.6525	124.322
$120^e$	8.1279	5.9461	8.6546	124.258
$131^e$	8.1356	5.9486	8.6568	124.197
$143^d$	8.1433	5.9512	8.6594	124.128
$153^e$	8.1508	5.9536	8.6610	124.066
$163^e$	8.1577	5.9559	8.6627	124.001
$173^e$	8.1647	5.9582	8.6644	123.933
$184^d$	8.1686	5.9617	8.6654	123.860
$195^e$	8.1799	5.9632	8.6678	123.772
$206^e$	8.1875	5.9657	8.6695	123.684
$217^e$	8.1952	5.9682	8.6711	123.591
$228^e$	8.2028	5.9707	8.6727	123.493
$239^d$	8.2128	5.9727	8.6745	123.388
$273^d$	8.2425	5.9806	8.6814	123.042
$296^d$	8.2606	5.9872	8.6816	122.671

<sup>a</sup>Reference 27.

<sup>b</sup>Reference 33.

<sup>c</sup>Reference 30.

<sup>d</sup>Reference 29.

<sup>e</sup>Fitting.

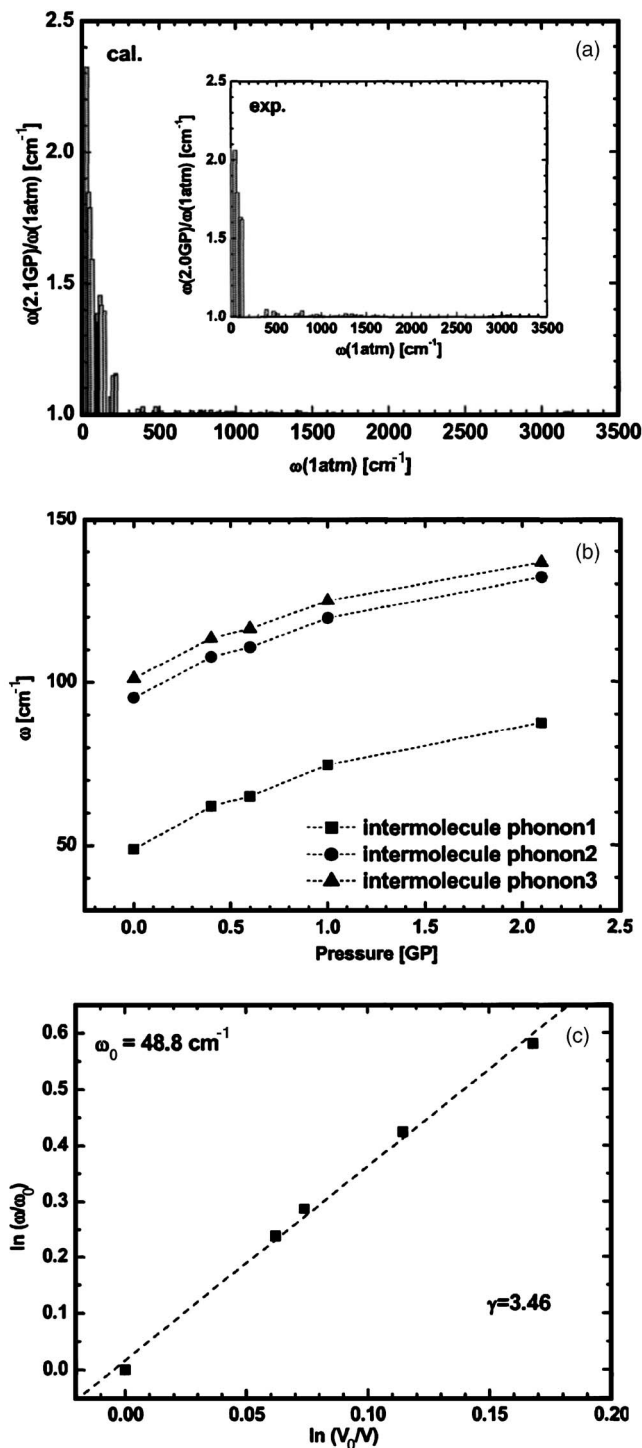


FIG. 2. (a) Ratio of the calculated phonon frequencies between 2.1 GPa with 1 atm. The experimental results (Ref. 34) are shown in the inset. (b) Pressure dependence of three intermolecular phonon frequencies. (c) Mode-Grüneisen parameter fit, which relate the phonon frequency with the unit-cell volume.

the constant  $\gamma$ . We found  $\gamma=3.46$ , which is in nice agreement with the measured value  $\gamma=3.6$ .<sup>35</sup> This further confirms the reliability of the electronic structure calculations. Even though the DFT is generally believed not able to describe the weak interaction, it turns out that the chosen PBE functional is very reasonable for our system.

Next, we look at how the electronic terms ( $\varepsilon$ 's) in the Holstein–Peierls model change with pressure. These are ob-

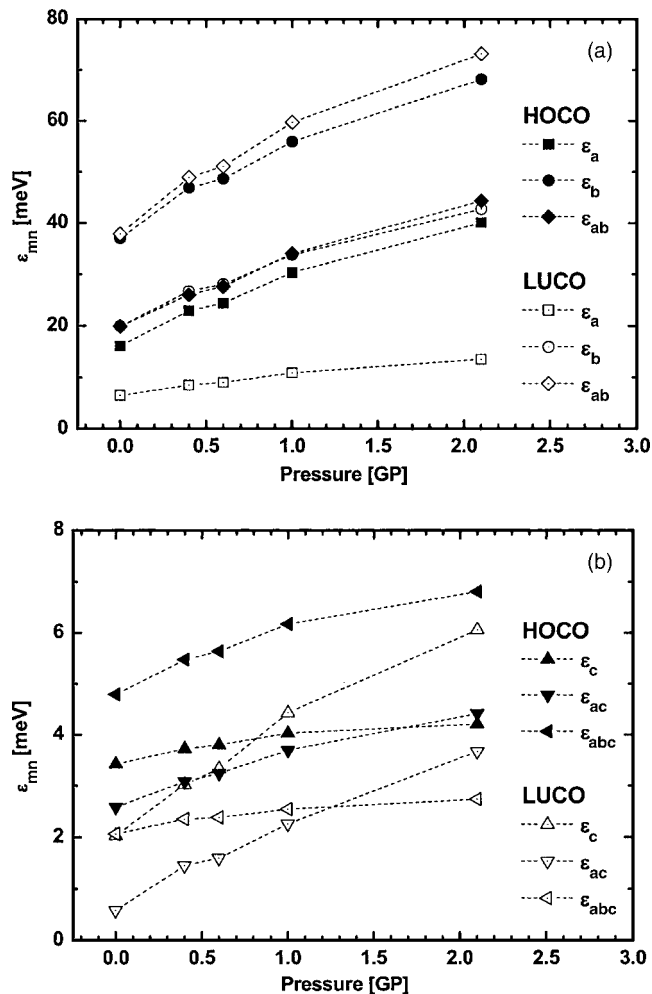


FIG. 3. The pressure-dependent transfer integrals of the (a) intralayer and (b) interlayer nearest neighbors.

tained through DFT band structures for the HOCO (hole) and LUCO (electron) bands fitted to the tight-binding model at each pressure value, see Figs. 3(a) and 3(b). The interlayer interactions are much weaker than the intralayer interactions in the naphthalene crystal,<sup>40,41</sup> so the charge transfer paths  $\{mn=a, b, ab\}$  have much larger contributions than the other directions.<sup>24,26(a)</sup> It is seen from Fig. 3(a) that the hopping terms are on average doubled when pressure is increased from ambient to 2.1 GPa.

We then look at the pressure-dependent electron- and hole-phonon coupling  $G$ . Figure 4(a) shows that both the electron-phonon and the hole-phonon coupling constants decrease as the pressure increases. It is interesting to note that the electron-phonon coupling constant is much larger than the hole-phonon one in naphthalene crystal. Therefore the former seems to decrease in a more remarkable way. In fact, both of them decrease about 40% when going from ambient to 2.1 Pa. In order to understand this disparity of electron and hole, let us take a look at the longitudinal optical phonon with the lowest frequency, which is found to be the most important one due to its large electron-phonon coupling constant and the large phonon occupation number at room temperature.<sup>26(a)</sup> We take the naphthalene dimer in the unit cell, and we focus on direction  $b$ . For this specific mode of

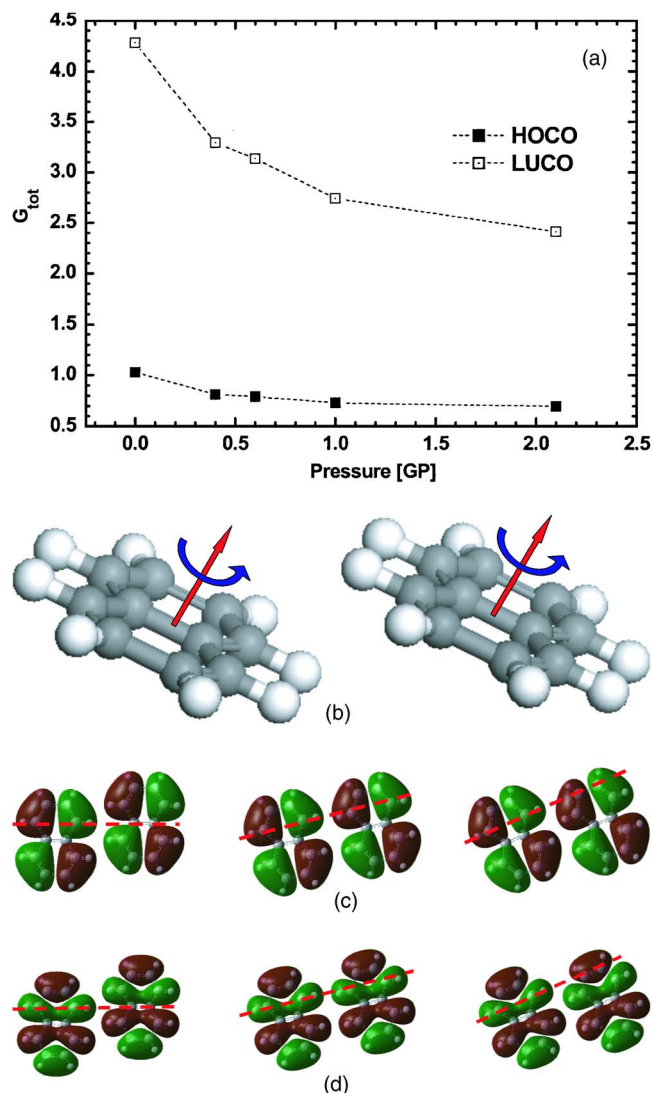


FIG. 4. (Color online) (a) The pressure dependence of the total hole-phonon and electron-phonon coupling constants. (b) Diagram of the rigid rotation of  $b$  dimer in the dominant mode. [(c) and (d)] Molecular dimer packing in the  $b$  direction with rotation around the perpendicular axis for  $0^\circ$ ,  $15^\circ$ , and  $25^\circ$  with orbital contour maps of (c) highest occupied molecular orbital and (d) lowest unoccupied molecular orbital. The dashed lines are used to indicate the relative positions of the two molecules along the perpendicular molecule plane. The left ends of the dashed lines are always fixed at the same position of the left naphthalene molecule, while the right ends of the lines sweep along the long axis of the right naphthalene.

$48.8 \text{ cm}^{-1}$ , the molecules themselves are found to be rigid, and they rotate along their perpendicular axes through the center of the molecules [see Fig. 4(b)]. Since there is a translational symmetry between  $b$  dimer due to our process of calculating phonon modes with only  $\Gamma$ -point, the rotation patterns for the two molecules in  $b$  dimer are the same. We plot in Figs. 4(c) and 4(d) the relative orientation of a naphthalene dimer under the relevant intermolecular rotation for  $0^\circ$ ,  $15^\circ$ , and  $25^\circ$ . The large rotation angle is an exaggeration for a guide of eyes. In calculation for the electron-phonon coupling constants, only a very tiny rotation angle is applied for the finite differentiation of Eq. (7). Upon rotating the molecule dimer according to this mode, we can find that the relative positions evidently change along the long axis of naphthalene molecule [shown by the dashed lines in Figs.

4(c) and 4(d), where left ends of the lines are fixed while the right ends sweep along the long axis of the right molecule]. Such rotation can result in change of relative phase of the two overlapping LUCO wavefunctions (electron) [the wavefunction along the dashed line in Fig. 4(c) has changed a lot during the rotation], but not for HOCO (hole). In other words, the change of the electron coupling of electrons will be larger than holes, namely, the electron-phonon coupling is much larger than the hole-phonon coupling in the naphthalene crystal.

In Fig. 5, we present the calculated hole and electron mobilities in the naphthalene single crystal as a function of pressure at room temperature in the  $a$ ,  $b$ , and  $c'$  directions. Here,  $c'$ -axis is normal to the  $ab$  plane of the naphthalene crystal. The nearly linear relationship between the hole mobility and the pressure is in good agreement with the experiment.<sup>22</sup> Furthermore, we find that the electron mobilities increase with pressure in a way much faster than the holes. To rationalize the different pressure behaviors of hole and electron, one may consider the following arguments: Among the five basic parameters in Eq. (2), only the transfer integrals and the electron-phonon coupling constants are different for electrons and holes. For simplicity, we use  $\mu \propto \varepsilon_{mn}^2 e^{-G_\lambda(P)}$  relationship to understand their main contributions to mobility. First the pressure dependences of the largest transfer integrals are almost the same for both holes and electrons, see Fig. 3(a). Therefore their contributions to the pressure dependence are nearly the same. Second, the decrease in the electron-phonon coupling is much larger than the hole-phonon coupling as the pressure increases [Fig. 4(a)], and then  $e^{-G_\lambda(P)}$  will increase much faster for electrons than holes. Therefore, the different pressure dependence can be fully rationalized from the coupling strengths of phonons with electrons and holes.

### C. Charge mobility and the temperature-dependent structure modification

The organic crystal structure changes with temperature. The experimental data of naphthalene crystal structures are available at temperatures  $T=5, 50, 92, 109, 143, 184, 239, 273, 296 \text{ K}$ ,<sup>29,30</sup> where for  $T=5$  and  $50 \text{ K}$ , the data are taken from the deuterated naphthalene  $\text{C}_{10}\text{D}_8$ , since its unit-cell volume is only about 0.3%–1.3% smaller than the  $\text{C}_{10}\text{H}_8$  due to the deuteration effect.<sup>30</sup> In order to get a smooth temperature dependence, we make appropriate interpolation among the experimental lattice constants for the whole temperature range 50–239 K by using analytic functions, see Fig. 6. The interpolating fittings are very successful since the correlation factors  $R$  are always close to 1. It should be noted that due to limited experimental data, such interpolation does not reveal the physical law governing the structure variation with respect to temperature. It only gives smooth fit. The lattice parameters including both the experimental and the interpolated data at ambient pressure are listed in Table I.

After taking the temperature-induced structure variation into account, the calculated temperature-dependent charge transport mobilities are shown in Fig. 7. Here, we only focus on the hole transport in the  $b$ -axis [Fig. 7(a)] and electron transport in the  $c'$ -axis [Fig. 7(b)], because (i) in naphtha-

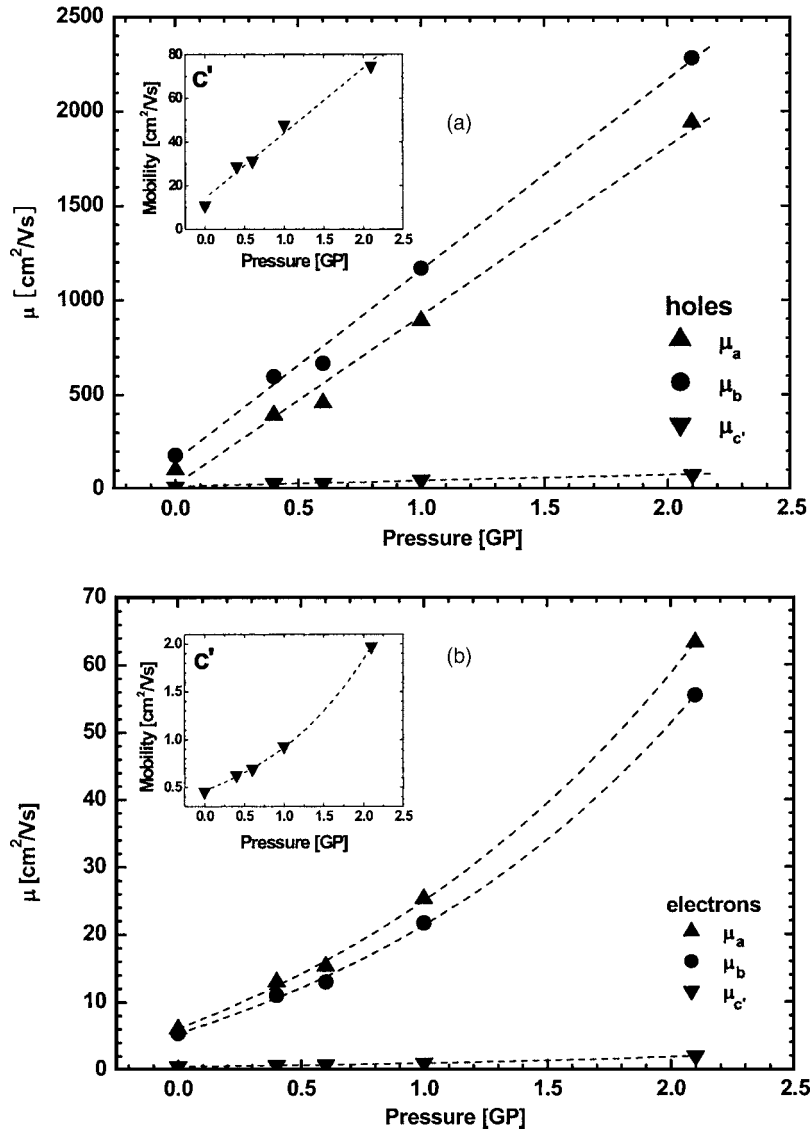


FIG. 5. The relationships between the hole and the electron mobilities and pressure.

lene, holes are the dominant carriers and the  $b$ -axis is the most important transport direction<sup>23,42</sup> and (ii) the band-hopping crossover occurs in the  $c'$  direction for electron transport which is of strong fundamental interest.<sup>43</sup> When compared to our previous results,<sup>26(a)</sup> we can make the following remarks.

- (i) The hole mobility decreases with temperature faster in high temperature range and thus overcomes our previous discrepancy with experiment above 60 K, which we had attributed to the possible thermal fluctuation effect.<sup>26(a)</sup> Now, with this natural structure dependence, the calculated temperature dependence of hole mobility is in much better agreement with the experiment.
- (ii) The band-hopping crossover transition temperature for the electron transport in the  $c'$ -axis is calculated to be around 153 K now, which is much larger than our previous result of about 23 K without considering the temperature-induced structure variation. This value agrees much better with the experimentally observed transition temperature between 100 and 150 K.

In Fig. 7, we also displayed the temperature dependences of hole and electron mobilities with fixed experimental lattices at various temperatures, since these dependences without considering the temperature-dependent structure modification can help us understand the intrinsic mechanism of the structure effect. The holes in the  $b$ -axis exhibit nearly the same bandlike transport, while the electron transport in the  $c'$ -axis remarkably changes from pure bandlike ( $T_{\text{fixed-lattice}} \leq 153$  K) to band-hopping crossover ( $T_{\text{fixed-lattice}} \geq 163$  K). Since the local and nonlocal mobilities in Eq. (3) approximately correspond to the bandlike and hopping parts, respectively, the different effects of structure to hole and electron transports can be well understood by analyzing the contributions of the local part  $\mu_{\text{local}}/(\mu_{\text{local}} + \mu_{\text{nonlocal}})$ , see Fig. 8. We can find that the local part is the main contribution to the hole transport in the  $b$ -axis over the whole temperature range 5–296 K. On the other hand, the contribution of the bandlike local part for electrons decreases from 100% at 5 K to about 20% at 296 K, thus band-hopping crossover should happen at a certain temperature. When transport begins to change from bandlike to band-hopping crossover, the mobility at that

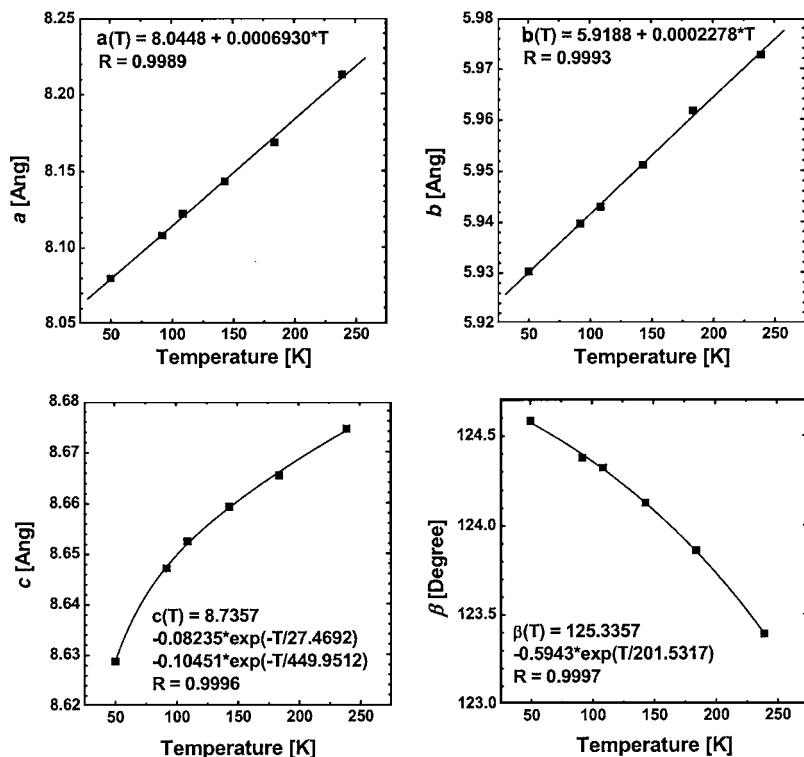


FIG. 6. Interpolating fits of crystal parameters  $a(T)$ ,  $b(T)$ ,  $c(T)$ , and  $\beta(T)$  with available experimental data (Refs. 29 and 30) over the range 50–239 K.

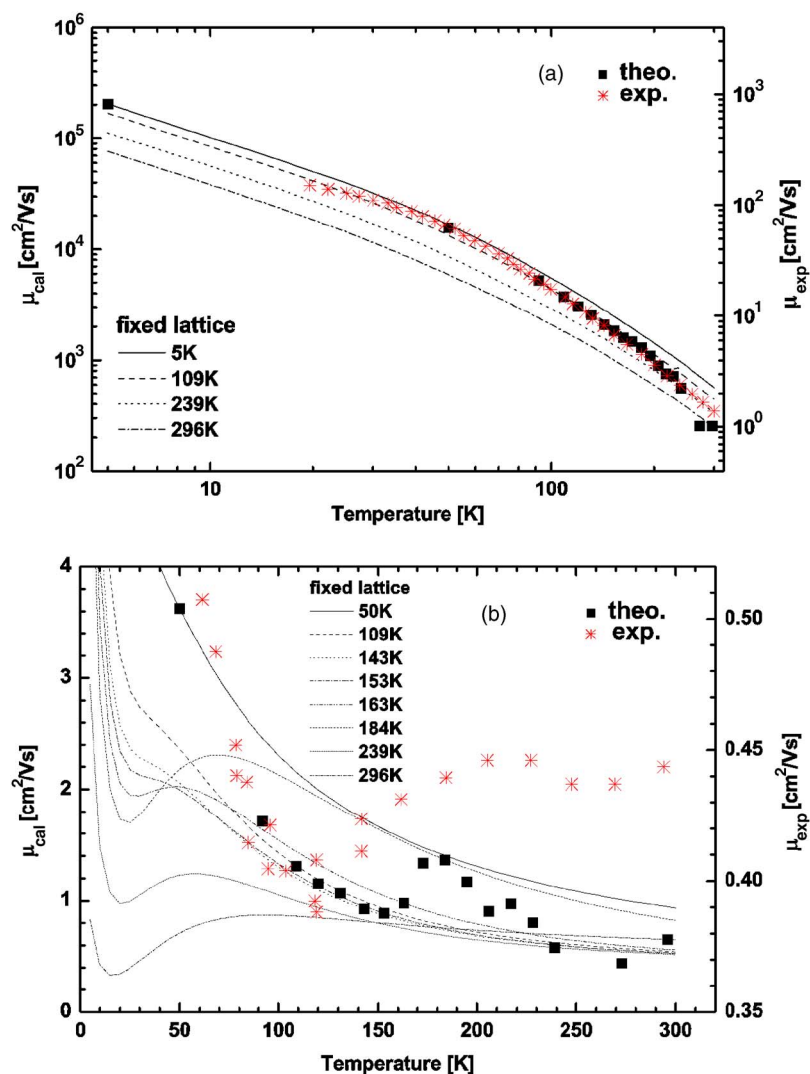


FIG. 7. (Color online) The calculated and experimental (Refs. 23, 42, and 43) results of the temperature-dependent mobilities of (a) hole in the  $a$ -axis and (b) electron in the  $c'$ -axis. The temperature-dependent mobilities with fixed lattice parameters are shown for comparison.

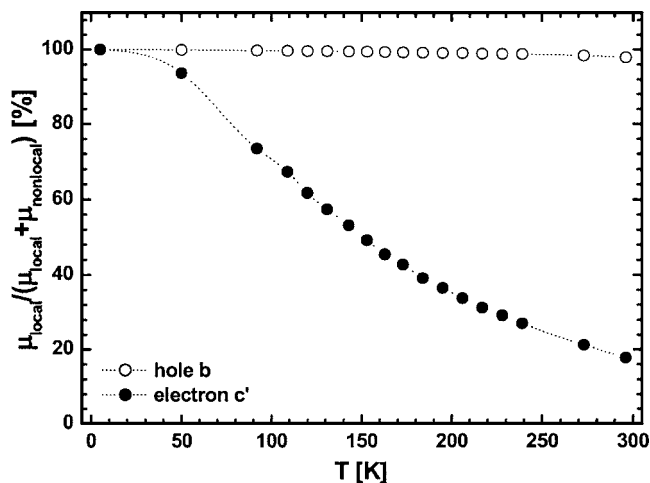


FIG. 8. The temperature dependence of the contributions of the bandlike local contribution for hole in the  $b$ -axis and for electron in the  $c'$ -axis.

temperature will suddenly increase. This temperature is just the band-hopping crossover transition temperature including the structure variation induced by temperature. According to our calculation, the crossover temperature is about 153 K.

Finally, we point out that present theoretical results overestimate the experimental mobilities by about two orders of magnitude. We attribute such discrepancy to the limit of the linear electron-phonon interaction assumed in the model and the neglect of the effect of acoustic phonons and the thermal fluctuation in the treatment of many-body effects.<sup>25</sup> In addition, our choice of inhomogeneous line broadening factor is very small to exclude disorders since we aim to study the temperature dependence of the charge transport in the ultra-pure crystal. However, the density of chemical and physical defects in single crystals has been seen in experiments.<sup>23,42</sup> A large broadening factor certainly will largely decrease the calculated mobility. Unfortunately, the treatment of these scattering processes is far from satisfaction which is beyond our present model, and detailed consideration of the effect may be quite complex in the systems due to the presence of static defects and disorder.<sup>25</sup>

Charge localization effect due to thermal fluctuation at growing temperature has been recently considered by Troisi and co-workers.<sup>18,19,44</sup> They got the decreased mobilities with temperature just like the transport in the  $b$ -axis for holes in Fig. 7(a), but the origins are obviously different from ours. Under our model, the intermolecular vibrational modes are found to be essential to scatter the electron/hole transport. These also cause bandwidth narrowing.<sup>24</sup> However, in deriving an effective one-body Hamiltonian from the original Holstein–Peierls mode, after the canonical transformation, the renormalized electronic terms, which contain infinite orders of electron-phonon couplings, are replaced by a thermal average.<sup>24,25</sup> The major drawback lies in the thermal average which makes the many-body problem tractable. But doing this, thermal fluctuation effect is neglected. The temperature enters in the phonon occupation distribution<sup>26(a)</sup> and temperature-dependent lattice variation in the present work. The bandwidth narrowing effect is contained, but not to the scale of complete localization of polaron. However, we note

that from Troisi's molecular dynamics simulation and the subsequent DFT calculations for the electron coupling terms, the fluctuations of  $\epsilon$ 's are in the same magnitude as  $\epsilon$ 's themselves. For the one-dimensional system, any disorder would cause complete localization. Such large fluctuation is not expected for a three-dimensional closely packed molecular crystal. The fluctuation effects should be further incorporated in the Holstein model study. After all, the projection to tight-binding model can only be done for simple molecules, which strongly limit the application scope of this method. All these need further studies to achieve a more satisfied quantitative description. Nevertheless, the present study does preliminarily reveal the pressure and temperature-induced structure modifications to the electron-phonon couplings and the mobility.

#### IV. CONCLUSION

In summary, we have investigated the pressure- and temperature-dependent mobilities in the naphthalene crystal by using DFT-projected Holstein–Peierls model. It is found that the pressure increases the phonon frequency, much more for the low-frequency phonons than for high-frequency ones, and lowers the electron-phonon coupling strengths. A nearly linear relationship between hole mobility and pressure has been reproduced from first-principles calculations. Besides, after considering the structure variation induced by temperature, the temperature-dependent mobilities of both holes and electrons have been found to much better agree with the experiments; especially, the band-hopping crossover temperature for the electron transport in the  $c'$ -axis is calculated to be 153 K, which is in nice agreement with the experimental result of between 100 and 150 K, while previous result gave only 23 K.

#### ACKNOWLEDGMENTS

This work is supported by the Ministry of Science and Technology of China (Grant Nos. 2002CB613406, 2006CB806200, and 2006CB0N0100) and NSFC, as well as the Chinese Academy of Sciences.

- <sup>1</sup>V. I. Adamovich, S. R. Cordero, P. I. Djurovich, A. Tamayo, M. E. Thompson, B. W. D'Andrade, and S. R. Forrest, *Org. Electron.* **4**, 77 (2003).
- <sup>2</sup>H. E. Katz, *J. Mater. Chem.* **7**, 369 (1997).
- <sup>3</sup>G. Horowitz, *Adv. Mater. (Weinheim, Ger.)* **10**, 365 (1998).
- <sup>4</sup>H. E. Katz and Z. Bao, *J. Phys. Chem. B* **104**, 671 (2000).
- <sup>5</sup>C. D. Dimitrakopoulos and P. R. L. Malenfant, *Adv. Mater. (Weinheim, Ger.)* **14**, 99 (2002).
- <sup>6</sup>H. Spanggaard and F. C. Krebs, *Sol. Energy Mater. Sol. Cells* **83**, 125 (2004).
- <sup>7</sup>W. Ma, C. Yang, X. Gong, K. Lee, and A. J. Heeger, *Adv. Funct. Mater.* **15**, 1617 (2005).
- <sup>8</sup>V. Coropceanu, J. Cornil, D. A. da Silva Filho, Y. Olivier, R. Silbey, and J. L. Brédas, *Chem. Rev. (Washington, D.C.)* **107**, 926 (2007).
- <sup>9</sup>M. E. Gershenson, V. Podzorov, and A. F. Morpurgo, *Rev. Mod. Phys.* **78**, 973 (2006).
- <sup>10</sup>C. Reese and Z. Bao, *Mater. Today* **10**, 20 (2007).
- <sup>11</sup>T. Holstein, *Ann. Phys. (N.Y.)* **8**, 343 (1959).
- <sup>12</sup>R. W. Munn and R. Silbey, *J. Chem. Phys.* **83**, 1854 (1985).
- <sup>13</sup>V. M. Kenkre, J. D. Anderson, D. H. Dunlap, and C. B. Duck, *Phys. Rev. Lett.* **62**, 1165 (1989).
- <sup>14</sup>K. Hannewald and P. A. Bobbert, *Appl. Phys. Lett.* **85**, 1535 (2004).
- <sup>15</sup>R. A. Marcus, *J. Chem. Phys.* **24**, 966 (1956).

- <sup>16</sup>N. S. Hush, *Trans. Faraday Soc.* **57**, 557 (1961).
- <sup>17</sup>J. Jortner, *J. Chem. Phys.* **64**, 4860 (1976).
- <sup>18</sup>A. Troisi and G. Orlandi, *Phys. Rev. Lett.* **96**, 086601 (2006).
- <sup>19</sup>A. Troisi, *Adv. Mater. (Weinheim, Ger.)* **19**, 2000 (2007).
- <sup>20</sup>Z. Rang, A. Haraldsson, D. M. Kim, P. P. Ruden, M. I. Nathan, R. J. Chesterfield, and C. D. Frisbie, *Appl. Phys. Lett.* **79**, 2731 (2001).
- <sup>21</sup>D. A. Dows, L. Hsu, S. S. Mitra, O. Brafman, M. Hayek, W. B. Daniels, and R. K. Crawford, *Chem. Phys. Lett.* **22**, 595 (1973).
- <sup>22</sup>Z. Rang, M. I. Nathan, P. P. Ruden, V. Podzorov, M. E. Gershenson, C. R. Newman, and C. D. Frisbie, *Appl. Phys. Lett.* **86**, 123501 (2005).
- <sup>23</sup>N. Karl, *Synth. Met.* **133**, 649 (2003).
- <sup>24</sup>K. Hannewald, V. M. Stojanović, J. M. T. Schellekens, P. A. Bobbert, G. Kresse, and J. Hafner, *Phys. Rev. B* **69**, 075211 (2004).
- <sup>25</sup>K. Hannewald and P. A. Bobbert, *Phys. Rev. B* **69**, 075212 (2004).
- <sup>26</sup>(a) L. J. Wang, Q. Peng, Q. K. Li, and Z. Shuai, *J. Chem. Phys.* **127**, 044506 (2007); (b) X. D. Yang, Q. K. Li, and Z. Shuai, *Nanotechnology* **18**, 424029 (2007).
- <sup>27</sup>F. R. Ahmed and D. W. J. Cruickshank, *Acta Crystallogr.* **5**, 852 (1952).
- <sup>28</sup>A. P. Ryzhenkov and V. M. Kozhin, *Sov. Phys. Crystallogr.* **12**, 943 (1968).
- <sup>29</sup>C. P. Brock and J. D. Dunitz, *Acta Crystallogr., Sect. B: Struct. Crystallogr. Cryst. Chem.* **38**, 2218 (1982).
- <sup>30</sup>E. Baharic and G. S. Pawley, *Acta Crystallogr., Sect. A: Cryst. Phys., Diffr., Theor. Gen. Crystallogr.* **38**, 803 (1982).
- <sup>31</sup>J. F. J. Jordan, A. Axmann, H. Egger, and J. Kalus, *Phys. Status Solidi A* **71**, 457 (1982).
- <sup>32</sup>R. G. D. Valle, E. Venuti, and A. Brillante, *Chem. Phys.* **198**, 79 (1995).
- <sup>33</sup>F. P. A. Fabbiani, D. R. Allan, S. Parsons, and C. R. Pulham, *Acta Crystallogr., Sect. B: Struct. Sci.* **62**, 826 (2006).
- <sup>34</sup>M. Nicol, M. Vernon, and J. T. Woo, *J. Chem. Phys.* **63**, 1992 (1975).
- <sup>35</sup>W. Häfner and W. Kiefer, *J. Chem. Phys.* **86**, 4582 (1987).
- <sup>36</sup>S. C. Capelli, A. Albinati, S. A. Mason, and B. T. M. Willis, *J. Phys. Chem. A* **110**, 11695 (2006).
- <sup>37</sup>G. Kresse and J. Hafner, *Phys. Rev. B* **47**, 558 (1993); **49**, 14251 (1994); G. Kresse and J. Furthmüller, *ibid.* **54**, 11169 (1996).
- <sup>38</sup>Y. L. Page and P. Saxe, *Phys. Rev. B* **65**, 104104 (2002).
- <sup>39</sup>E. F. C. Byrd, G. E. Scuseria, and C. F. Chabalowski, *J. Phys. Chem. B* **108**, 13100 (2004).
- <sup>40</sup>J. Cornil, D. Beljonne, J. P. Calbert, and J. L. Brédas, *Adv. Mater. (Weinheim, Ger.)* **13**, 1053 (2001).
- <sup>41</sup>J. L. Brédas, D. Beljonne, V. Coropceanu, and J. Cornil, *Chem. Rev. (Washington, D.C.)* **104**, 4971 (2004).
- <sup>42</sup>N. Karl, in *Organic Semiconductors*, Landolt Bornstein, New Series, Group III, Vol. 17, edited by K.-H. Hellwege and O. Madelung (Springer, Berlin, 1985), pp. 106–218.
- <sup>43</sup>L. B. Schein, C. B. Duke, and A. R. McGhie, *Phys. Rev. Lett.* **40**, 197 (1978).
- <sup>44</sup>A. Troisi and G. Orlandi, *J. Phys. Chem. A* **110**, 4065 (2006).